Phase Unwrapping in Digital Holography based on SRDU-Net

Yuan Chen[1,2,*], Quan Wang[3], Guangming Zhang[4], Peichao Li[3], Yuhui Fan[3], Zhongyang Wang[3], Ming Dong[2,3]

1College of Sciences, Xi'an University of Science and Technology, Xi'an, Shaanxi, 710054, China

2Shaanxi Key Laboratory of Mine Electromechanical Equipment Intelligent Detection and Control, Xi'an University of Science and Technology, Xi'an, Shaanxi, 710054, China

3College of Mechanical Engineering, Xi'an University of Science and Technology, Xi'an, Shaanxi,710054, China

4General Engineering Research Institute, School of Engineering, Faculty of Engineering and Technology, Liverpool John Moores University, Byrom Street, L3 3AF, United Kingdom

**Email: chenyuan1030@126.com*

Abstract: In digital holographic measurement, the hologram phase is extracted using an inverse tangent function, resulting in a wrapped phase that is constrained to be $(-\pi, \pi]$. However, the phase contains the height information of the object, which is crucial for accurate measurement of the object contour. Therefore, a digital holographic phase unwrapping method based on SRDU-Net (Separable-Residual-Dense-Inverted U-Net) is proposed in this paper. The SRDU-Net network is constructed by introducing depth-separable convolution, inverted residuals and dense blocks with U-Net as the network framework to achieve high-precision hologram phase recovery. This network adopts depth-separable convolution instead of traditional convolution, combines the inverse residual connection to construct a lightweight convolution structure, and defines dense blocks with this structure to form a lightweight grouped deep convolution network. Meanwhile, the Leaky ReLU activation function is used to introduce the learning rate mechanism to optimize the network parameters with Huber and MSE (mean square error) as the combined loss function. The simulated phase dataset is used to train the network, the trained network model is tested for speckle noise immunity, and phase unwrapping experiments are performed on the collected holograms of the test samples. The results show that SRDU-Net improves the SSIM by 0.1% and reduces the RMSE by 86% over Res-UNet (Residual-UNet). Therefore, the proposed method can realize high-precision recovery of digital holographic wrapped phases, and has a good robustness to phase unwrapping of holograms containing a high degree of speckle noise.

Keywords: digital holography; phase unwrapping; depth-separable convolution; inverted residuals; dense block

1.Introduction

Digital holographic microscopy [1, 2] is a powerful three-dimensional imaging technology based on the principle of light interference. It uses a CCD camera to record a hologram containing the wavefront information of the measured object, and uses a computer to perform numerical reconstruction to obtain the phase and amplitude information of the measured object, and then obtain the three-dimensional morphology of the object. Due to its advantages of non-contact, calibration-free and quantitative measurement, it has been widely used in optics, radar, medical imaging and other fields [3-5]. When the phase information is extracted from the holograms using an inverse tangent function, the phase is bounded between $(-\pi, \pi]$, which causes a "wrapping" phenomenon, i.e., the phase value varies cyclically within a certain range, which cannot directly reflect the true physical properties [6]. Therefore, the phase unwrapping method is required to remove the "wrapping" phenomenon to recover the true phase information.

In recent years, many phase unwrapping methods have been proposed, which can be divided into spatial phase unwrapping (SPU) and temporal phase unwrapping (TPU) according to different principles and application scenarios [7, 8]. SPU is mainly to find an optimal phase unwrapping path in the phase map, i.e. phase unwrapping in the same space. This method performs the unwrapping operation according to the phase difference between a certain point and its neighbors. It needs only one phase map to complete, but the phase unwrapping operation of each point is related to the surrounding neighbors. Representative algorithms include diamond-type SPU, curtain-type SPU, least squares SPU, quality-guided SPU, branch-cut SPU, etc. Diamond-type SPU tends to accumulate phase errors during phase unwrapping, resulting in phase unwrapping errors. Therefore, additional structured light is needed to confirm the stripe order to avoid phase error accumulation, such as grey code, binary grating, and so on [9]. The curtain-type SPU is guided by the residual template generated by the closed curve method and the binary template generated by the Otsu threshold method, and the phase unwrapping is performed by the upper and lower symmetry and the left and right symmetry around the starting point [10]. The least squares SPU performs phase unwrapping by transforming the phase unwrapping problem into the problem of minimizing the error function that measures the difference between the unwrapped phase value and the measured phase value. However, this method often has obvious unwrapping errors. Discrete cosine transform least square (DCT-LS) combines least squares SPU and frequency domain processing technology to transform data from the spatial domain to the frequency domain by discrete cosine transform. The phase unwrapping error is then minimized by solving the Poisson equation [11]. Quality-guided SPU generates a quality map based on the fringe density to guide the phase unwrapping [12]. Branch-cut SPU generates a residual map by connecting the residual points, thereby guiding the phase unwrapping path to avoid areas with large residuals. The famous traditional branch-cut is Goldstein's branch-cut (GBC) [13].

TPU is based on time series of two or more-phase maps of different frequencies obtained at different times at the same position to be unwrapped. In the process of temporal phase unwrapping, the phase of each point is only related to the phase points at the same position on the phase map of different frequencies, and has nothing to do with its adjacent points. Representative algorithms include fringe amplitude encoding TPU, binary encoding TPU, phase encoding TPU, phase shift encoding TPU, etc. The fringe amplitude encoding TPU directly encodes different fringe amplitudes of different periods in the sinusoidal phase shift mode to generate space division multiplexing composite sinusoidal phase-shifting patterns, and inverts the absolute phase by quantifying the fringe amplitude into four encoding strategies [14]. Binary coding TPU needs to project a series of binary coding patterns on the surface of the object to obtain the surface information of the object, but this method has many interferences. Wang et al. [15] proposed a spatial binary coding (SBC), which achieves absolute phase recovery by using binary N-bit coding for each stripe order in sinusoidal phase shift patterns, and improves the accuracy of recovery. However, SBC will lead to an imbalance between the periodic divisions and codewords. Wu et al. [16] presented a large codeword orthogonal spatial binary coding. By increasing the orthogonal direction of spatial multiplexing by one dimension, the codeword expansion is realized and the balance between the low-period division and the codeword is maintained. Phase coding TPU encodes the phase information into the coding pattern and then parses the coding pattern, but it requires a large number of auxiliary patterns. Ruan et al. [17] proposed a spatial ternary phase coding method. In the case of only one auxiliary coding patterns, the robustness of the decoding is guaranteed and a large codeword space is realized. This method divides the stripe order into multiple segments, and then uses an arccosine operation to encode three different phase values in each segment to realize the ternary coding of the stripe order. Phase shift encoding TPU is designed to mark the known phase offset of the position and order of the fringes, but the wrapped phase and the fringe order will be periodically displaced. Li et al. [18] proposed a two-stage unwrapping method based on phase shift encoding, which reduces the number of fringe projections. Only four composite fringe patterns are required to directly analyze the wrapped phase and fringe order.

In summary, how to choose the appropriate unwrapping method for different application scenarios is a problem that needs to be addressed. Aiming at the shortcomings of the above unwrapping algorithms, deep learning-based unwrapping algorithms have been applied in the field of digital holographic measurements, which are mainly divided into three categories: deep learning regression methods, deep learning wrap-count methods, and deep learning denoising methods. Deep learning regression methods directly fit the true phase of the target data by fully learning the mapping relationship between the wrapped phase and the true phase, such as PHU-Net [19], PU-GAN [20], BCNet [21], and so on. Deep learning wrap-count methods predict the wrap-counts of the target data based on the input the wrapped phases and wrap-counts by a network model, which is then unwrapped the phases by traditional unwrapping algorithms using the image segmentation models, such as phaseNet [22], phaseNet2.0 [23], and so on. Deep learning denoising methods, which are less used currently, denoise the real and imaginary parts of the image data using a network model and then unwrap the phases using traditional phase unwrapping methods, such as the ResNet network [24]. Wang et al. [25] summarized and comparatively analyzed deep learning-based phase unwrapping methods in recent years, and indicated that the robustness of deep learning based denoising methods is much lower than the previous two methods. Deep learning wrap-count methods require two steps to achieve, making them much more complex and less efficient than deep learning regression methods. They proposed a Res-UNet network based on the U-net structure, which solves the issues of gradient disappearance and gradient dispersion network, as well as the low network learning rate and accuracy of the deep learning regression method by adding jump connections and introducing residual learning with the network. However, Res-UNet has some limitations in terms of model fitting capability and model computation, such as more time-consuming model training, larger training loss, and so on.

Aiming to the drawbacks of the above methods, we propose a phase unwrapping method based on the SRDU-Net using the U-Net [26] network framework. A large amount of simulated phase data is randomly generated by the Gaussian function superposition (GFS) and random matrix enlargement (RME) to form a dataset for network training and testing. Different levels of speckle noise are added to the test samples to verify the immunity of the network to speckle noise. A reflective off-axis digital holographic optical path system is constructed to collect the holograms of test samples for experimental testing, and the results are compared with those of other methods to validate the proposed method.

2.Principles and Methods

Phase unwrapping aims to recover the continuity of the phase information by adding or subtracting appropriate multiples of 2π to recover physically continuous phase changes, thus eliminating phase jumps. The true phase can be estimated by the following equation [27]:

$$\delta = \varphi + 2\pi k \tag{1}$$

where δ is the true phase, φ is the wrapped phase, and k is an integer.

2.1. SRDU-Net Network Unwrapping Process

Deep learning is used to realize phase unwrapping by fitting a multiple of 2π with per-cycle weights of network training to obtain a mapping relationship between the wrapped phase and the true phase. The flowchart of the phase unwrapping using the SRDU-Net network is shown in Fig. 1. The green part represents the functional relationship between the wrapped phase and the true phase; the wrapped phase is used as the input, and the prediction result is obtained by SRDU-Net training. Then the network parameters are adjusted by calculating the difference between the predicted phase and the true phase using the loss function, so as to optimize the parameters of the SRDU-Net network model.

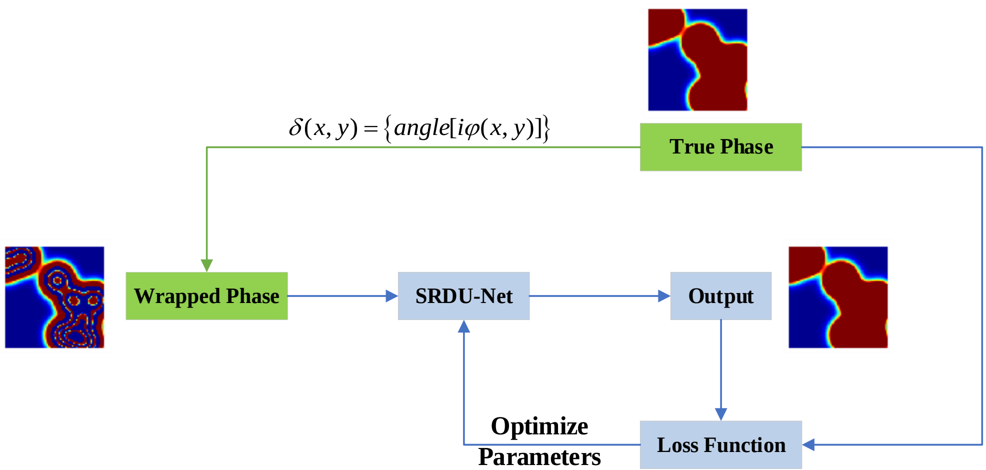

Fig.1. The flowchart of the SRDU-Net network unwrapping.

2.2. SRDU-Net Network Model

The SRDU-Net framework adopts the symmetric structure of U-Net and establishes direct connections between feature maps at different levels through skip connections, which makes the network more representational, better captures and preserves image details and contextual information in the image, effectively mitigates the vanishing gradient problem, and is easier for network training, thus accelerating the convergence speed of the network and improving the stability of the training process. The network framework of SRDU-Net is shown in Fig. 2, which is a 5-layer U-shaped structure. The left side is the down-sampling part, which is composed of SRDBlock and max pooling layer, and the right side is the up-sampling part, which is composed of deconvolution layer and SRDBlock. The tensor splicing operation is added between the two layers to fuse the features.

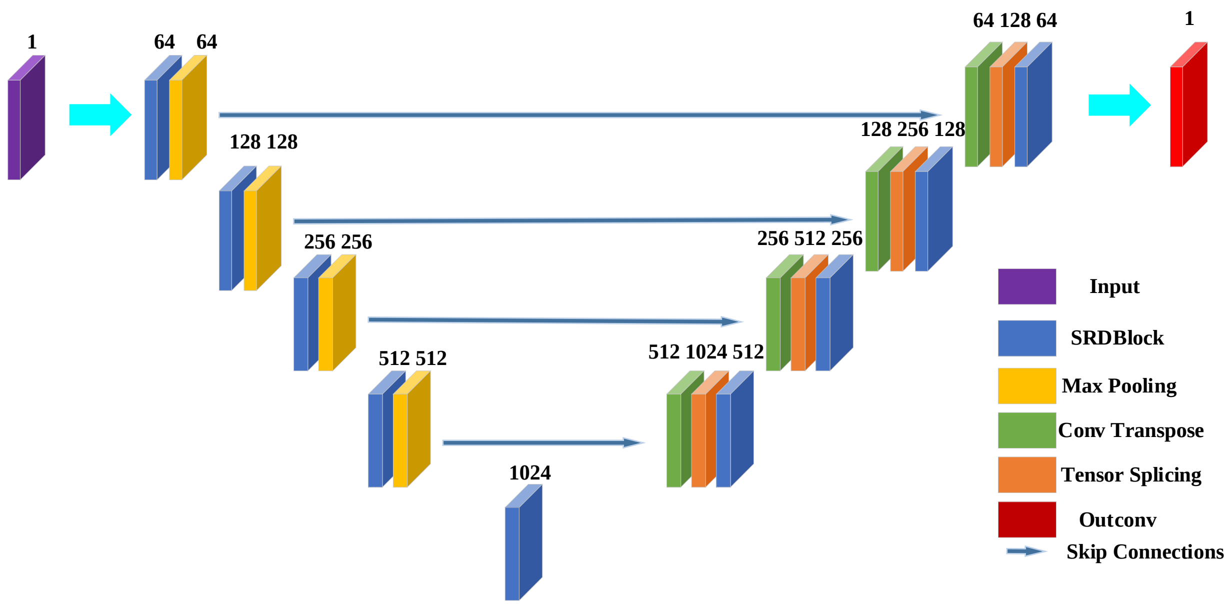

Fig.2. Schematic diagram of SRDU-Net network structure.

The numbers labeled in Fig. 2 represent the number of channels per network layer. Table 1 gives the hierarchies of the SRDU-Net network model.

In Table 1, the numbers in the first column represent the network layer, the numbers in the second and fourth columns represent the number of channels corresponding to the input and output of each network layer, and the characters in the third column represent the operation modules taken by each network layer.

Table 1. The hierarchies of the SRDU-Net network.

Layer	Input	Operator	Output
1	1	DownBlock	64
2	64	DownBlock	128
3	128	DownBlock	256
4	256	DownBlock	512
5	512	SRDBlock	1024
6	1024	UpBlock	512
7	512	UpBlock	256
8	256	UpBlock	128
9	128	UpBlock	64
10	64	Outconv	1

The convolution operation in the SRDU-Net framework is performed by the defined DepthwiseSeparableBlock, which adopts depthwise convolution and pointwise convolution to extract features at a deeper level while improving the efficiency and reducing the computational cost and storage requirements. As higher-level features are extracted, it results in heavier computational load and longer computation time. Therefore, inverted residual connection is used on the convolution results to reduce the computational load of the network, thus constructing a lightweight convolutional structure. Depthwise convolution applies a convolution kernel of the corresponding channel for each output channel of the input data, thus performing convolution operations on individual channels so that each channel only contains the features of that channel with a convolution kernel size of 3×3. Pointwise convolution performs a dot product operation on the output of depthwise convolution using a 1×1 convolution, which linearly combines features from different channels. Depthwise convolution adopts ReLU as the activation function, which has the advantages of simple computation and the ability to mitigate the vanishing gradient problem. Both depthwise convolution and pointwise convolution of the data are followed by batch normalization (BN) which speeds up the training process and improves the performance and stability of the model. The flowchart of the DepthwiseSeparableBlock is shown in Fig. 3.

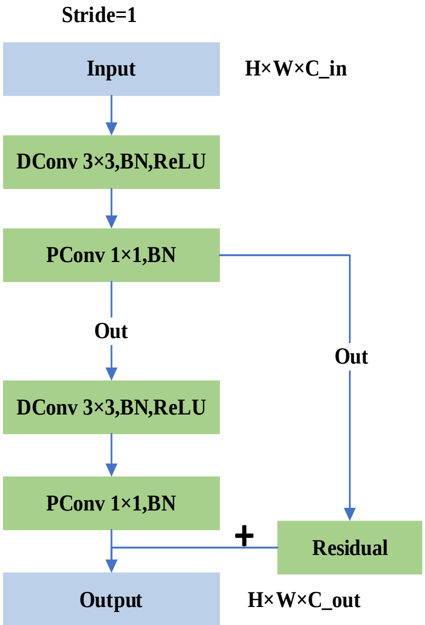

Fig.3. The flowchart of DepthwiseSeparableBlock. (DConv denotes Depthwise Convolution; PConv denotes Pointwise Convolution; BN denotes Batch Normalization)

To improve the training speed and accuracy of the SRDU-Net model, DenseBlock is defined by DepthwiseSeparableBlock to deepen the network level. DenseBlock integrates the extracted features, so that the model learns the advanced feature representation of the input data. The structure of DenseBlock is shown in Table 2, where Input represents the input channel, Output represents the output channel, and In_channels represents the number of input channels.

Table 2. DenseBlock.

Layer	Input	Operator	Output
1	In_channels	DepthwiseSeparableBlock	In_channels+1*32
2	In_channels+1*32	DepthwiseSeparableBlock	In_channels+2*32
3	In_channels+2*32	DepthwiseSeparableBlock	In_channels+3*32
4	In_channels+3*32	DepthwiseSeparableBlock	In_channels+4*32

In addition, to improve the learning capability of the SRDU-Net model, SRDBlock (Separable-Residual-Dense-Inverted Block) is defined based on DenseBlock, as shown in Fig. 4. In SRDBlock, the first layer is a 3×3 dimensionality ascending convolution layer, which sets the number of input channels to the number of output channels. The second layer is a DenseBlock, which performs data upscaling to learn advanced feature expressions. The final layer is a 1×1 dimensionality reduction convolution layer. The SRDBlock emphasizes the useful information learned by the model while suppressing useless features, and transforms the number of input channels to the desired number of output channels.

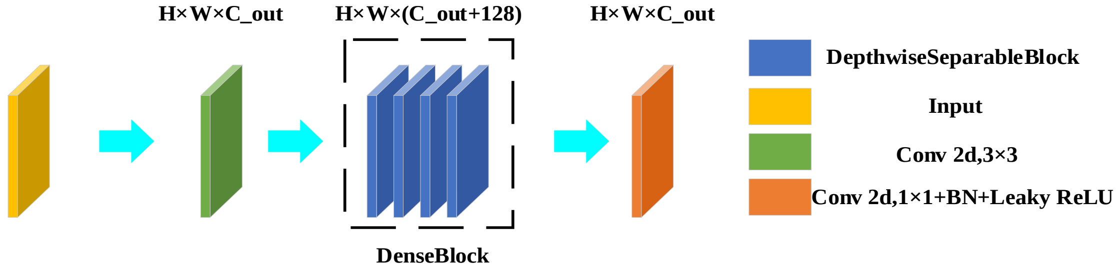

Fig.4. SRDBlock.

Leaky ReLU is used as the activation function employed in the dimensionality reduction convolution layer [28], which is a modified version of the linear unit. It maintains linearity in the non-negative range and introduces a small slope in the negative range, which is generally set to 0.01. This activation function has the advantages of ReLU and solves the issue of neurons inactivation when the input data is negative, which can be expressed by:

$$f(x) = \begin{cases} 0.01 * x, x < 0 \\ x, x \geq 0 \end{cases} \tag{2}$$

2.3. Loss Function

The loss function is crucial to the unwrapping accuracy in deep learning-based phase unwrapping methods. The loss function optimizes the network model by calculating the difference between the network output and the true value, thereby reducing the difference between the two. The smaller the value of the loss function, the better the fit of the network, and the better the robustness to phase noise, breakpoints and aliasing. As a fitting regression model, the loss function is selected from mean absolute error (MAE, L1 Loss), mean square error (MSE, L2 Loss), and Huber robust loss function [29] (SmoothL1 Loss). SmoothL1 Loss is an improvement on L1 Loss by introducing a smoothing function to reduce the influence of large differences, which is a loss function between MAE and MSE. When the error is small, the MSE of L2 Loss is used for SmoothL1 Loss; when the error is large, the MAE of L1 Loss is adopted. It has the following advantages: it has a better smoothness when the error is small, making it insensitive to outliers; it has a better gradient stability when the error is large, avoiding the gradient explosion.

The L2 Loss function expression is:

$$L2 = \frac{1}{n}\sum_{i=1}^{n}[y_i - f(x_i)]^2 \tag{3}$$

where y_i is the true value, $f(x_i)$ is the predicted value, and n is the number of samples.

The SmoothL1 Loss expression is:

$$SmoothL1 = \begin{cases} \frac{1}{2}[y - f(x)]^2, x < 0 \\ \sigma|y - f(x)| - \frac{1}{2}\sigma^2, x \geq 0 \end{cases} \tag{4}$$

where *y* is the true value, *f(x)* is the predicted value, and σ is a hyperparameter controlling the degree of smoothing of the Huber robust loss function.

If SmoothL1 Loss is used alone as the loss function for training, although the loss of the whole network is gradually stabilized, there will still be a sudden increase in the loss value at certain cycle nodes. Therefore, the loss function used in this paper is a combination function, which linearly combines SmoothL1 Loss with L2 Loss through weighted assignment, so as to avoid loss fluctuations caused by excessive errors. Its expression is as follows:

$$L_{total} = w_1 * SmoothL1 + w_2 * L2 \tag{5}$$

where w_1 and w_2 are the respective weight values, $w_1 + w_2 = 1$. The loss function weights are automatically adjusted by network training, and the model is best trained when w_1=0.7 and w_2=0.3.

2.4. Simulated Dataset for Network Training and Testing

2.4.1 Simulated Dataset Generation

The methods for generating absolute phase data involving deep learning can be divided into four categories: Random matrix enlargement (RME) [30-32], Gaussian functions superposition (GFS) [33-35], Zernike polynomials superposition (ZPS) [36,37], and Real data reprocessing (RDR) [38,39]. RME obtains the absolute phase of various distributions by amplifying a small random matrix with random size and range. GFS obtains the absolute phase of various distributions by weighted superposition of multiple Gaussian functions with different mean and variance. ZPS obtains the absolute phase of various distributions by weighted superposition of Zernike polynomials of different orders. RDR uses traditional methods to obtain the absolute phase of the real sample.

SRDU-Net and Res-Net use the same set of simulated data for training and testing. The simulated data generation method is to randomly generate the absolute phase in two ways: RME and GFS in a 1:1 ratio. The RME parameters are as follows: the initial matrix size range is [-8,8], the phase height range is [10,40], and the Gaussian noise with a maximum standard deviation of 1 is added using a random function when generating the absolute phase. The GFS parameters are as follows: each Gaussian function is determined by a randomly selected center point and a fixed standard deviation. The standard deviation is 5, and the amplitude is 1. The random number range of the Gaussian function superposition is [1,10], and the phase height range is [0, *h*], and where *h* is determined by the random distribution of the generated data volume, which is divided into three different intervals, and the value range of *h* is [10,40]. A random noise with a standard deviation range of [0,1] is added when generating an absolute phase. After the absolute phase is generated by this method, the real and imaginary parts of the generated absolute phase are wrapped by the arctangent function to obtain the corresponding wrapped phase. Finally, the wrapped phase is used as the input, and the absolute phase is used as the ground-truth phase.

The generated phase image has a size of 128×128, the amount of training data is 20000 groups, and the amount of test data is 2000 groups.

2.4.2 Network training methods

In the network training, the input wrapped phase is iteratively fitted by the neural network to perform phase unwrapping, and the model fitting result is obtained. The network output result and the absolute phase are calculated based on the loss function, thereby reducing the model loss and improving the model fitting effect. 20000 sets of training data are used for network training, and are randomly divided into the training and verification sets at a ratio of 8:2. After the network training is completed, 2000 sets of test data are used to test the performance of the network.

The SRDU-Net network model is implemented using the Pytorch (Python 3.9) framework, and the network training and testing is performed on a computer with a 13th Gen Intel(R) Core (TM) i9-13900KF CPU, 32G RAM memory and NVIDIA GeForce RTX 4090 GPU.

3. Analysis of Network Training and Testing Results

3.1 Network Training and Testing

The SRDU-Net network is trained and tested using the above simulated dataset, and the results are compared with those of the Res-UNet network to verify its feasibility and effectiveness. The training parameters of the SRDU-Net network are set as follows: the batch size is 15, the learning rate in the Adam optimizer is 0.85 and iteratively updated with a multiple of 0.85 to reach 1×10^{-6} to stop the iteration, the convolution step is 1. After reaching 100 iterations, both of the above networks have reached convergence. The first epoch of the SRDU-Net training takes 82.912s, and the completion of the training takes 7742.944s. While the first epoch of the Res-UNet training takes

81.886s, and the completion of the training takes 7749.976s. Although SRDU-Net takes 1s longer than the first epoch of Res-UNet training, it takes 7s less than Res-UNet as a whole. And the comparative curves of the training and validation set losses for both networks are shown in Fig. 5.

From Fig. 5, it can be seen that the training and validation losses of the SRDU-Net network are significantly lower than that of Res-UNet, indicating that it has a better training effect. The above testing set is used for unwrapping testing using the trained SRDU-Net and Res-UNet networks, and time-consuming are 27s and 32s, respectively. To quantitatively assess the performance of both networks, structural similarity index (SSIM) [40] and root mean square error (RMSE) [41] are adopted to evaluate the testing results.

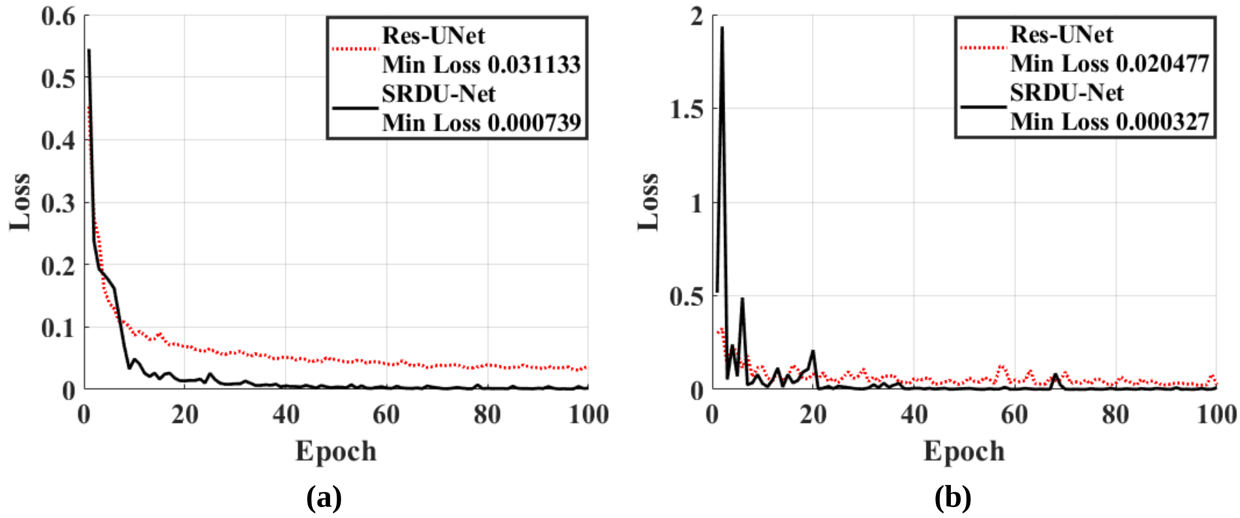

Fig. 5. Comparative curves of the losses for both networks. (a) training loss; (b) validation loss.

SSIM is a measure of the degree of structural similarity between the network outputs and the true phases, which is calculated by:

$$SSIM = \frac{(2\mu_x\mu_y + C_1)(2\sigma_{xy} + C_2)}{(\mu_x^2 + \mu_y^2 + C_1)(\sigma_x^2 + \sigma_y^2 + C_2)} \tag{6}$$

where μ is the phase mean, σ is the phase standard deviation, and C is a smaller constant to ensure that the denominator is non-zero.

RMSE is used to compute the square root of the mean square error between the network outputs and the true phases, serving as a measure to evaluate the error between the two, which is calculated as follows:

$$RMSE = \sqrt{\frac{\sum_{i=1}^{N}(y_i - y)^2}{N}} \tag{7}$$

where y_i is the network output and y is the true phase.

The SSIM and RMSE for the testing results of two network are shown in Fig. 6.

The mean value of SSIM for the Res-UNet network testing results is 0.99177, and the mean value of RMSE is 0.174970, while the mean value of SSIM for SRDU-Net network is 0.99280, which is 0.1% higher than that of Res-UNet. The mean value of RMSE for SRDU-Net network is 0.024515, which is 86.0% lower than that of Res-UNet. In addition, as depicted in Fig. 6, the values of two metrics of the testing results for the SRDU-Net network fluctuate within a small range, indicating better stability. Therefore, the overall performance of the SRDU-Net network is superior to that of the Res-UNet network.

To verify whether the fluctuation of metric values affects the results of the network output, three sets of samples are randomly selected from the above testing set to test the SRDU-Net network. The results are depicted in Fig. 7, and the values of SSIM and RMSE corresponding to Fig. 7 are shown in Table 3, which indicates that the SRDU-Net network achieves a good performance on phase unwrapping.

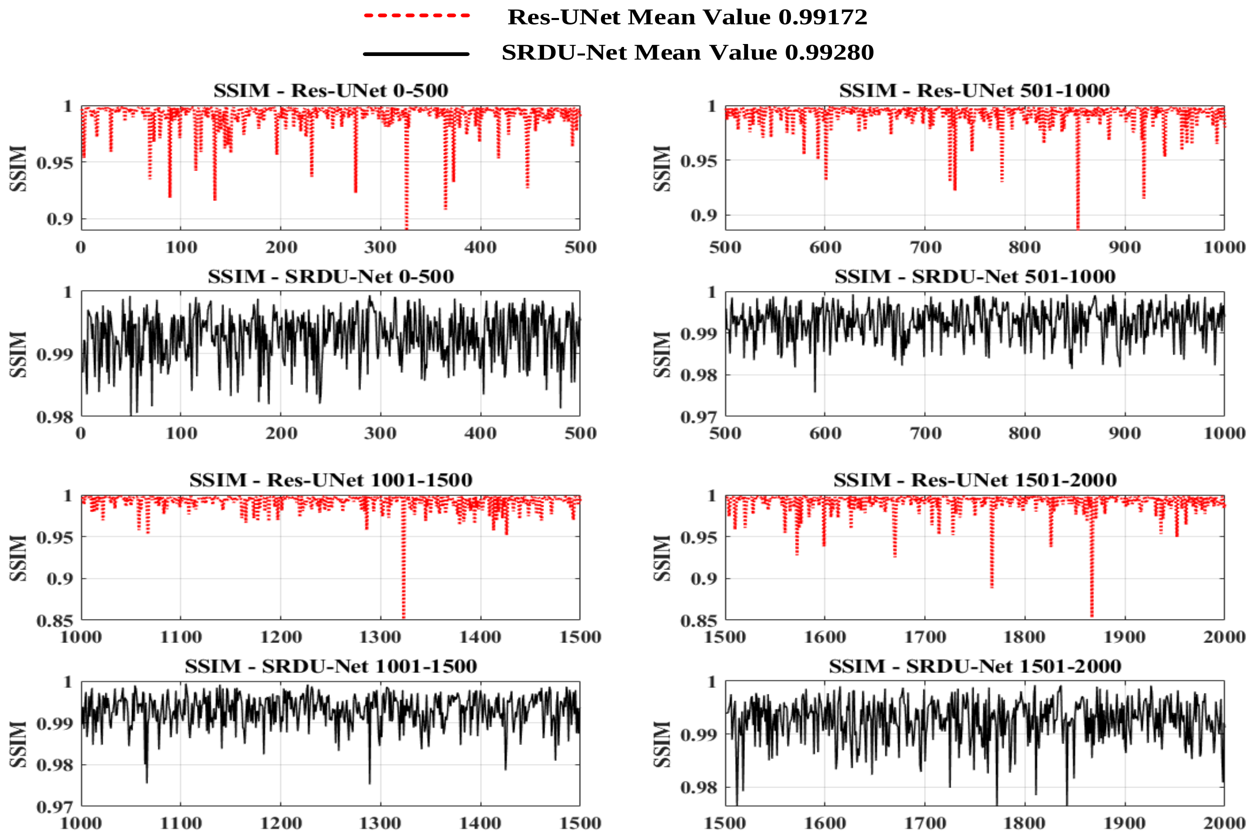

(a)

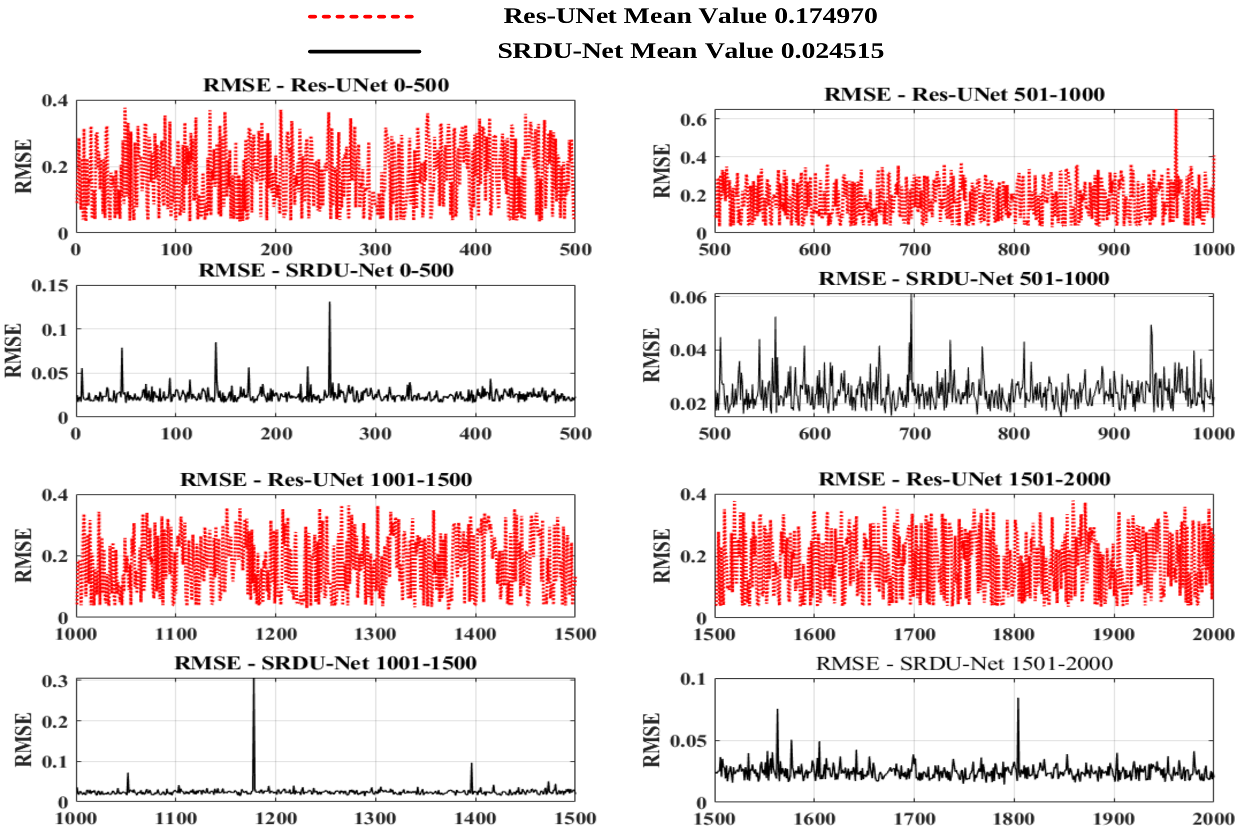

(b)

Fig. 6. Two metrics for the testing results of two network. (a) SSIM; (b) RMSE.

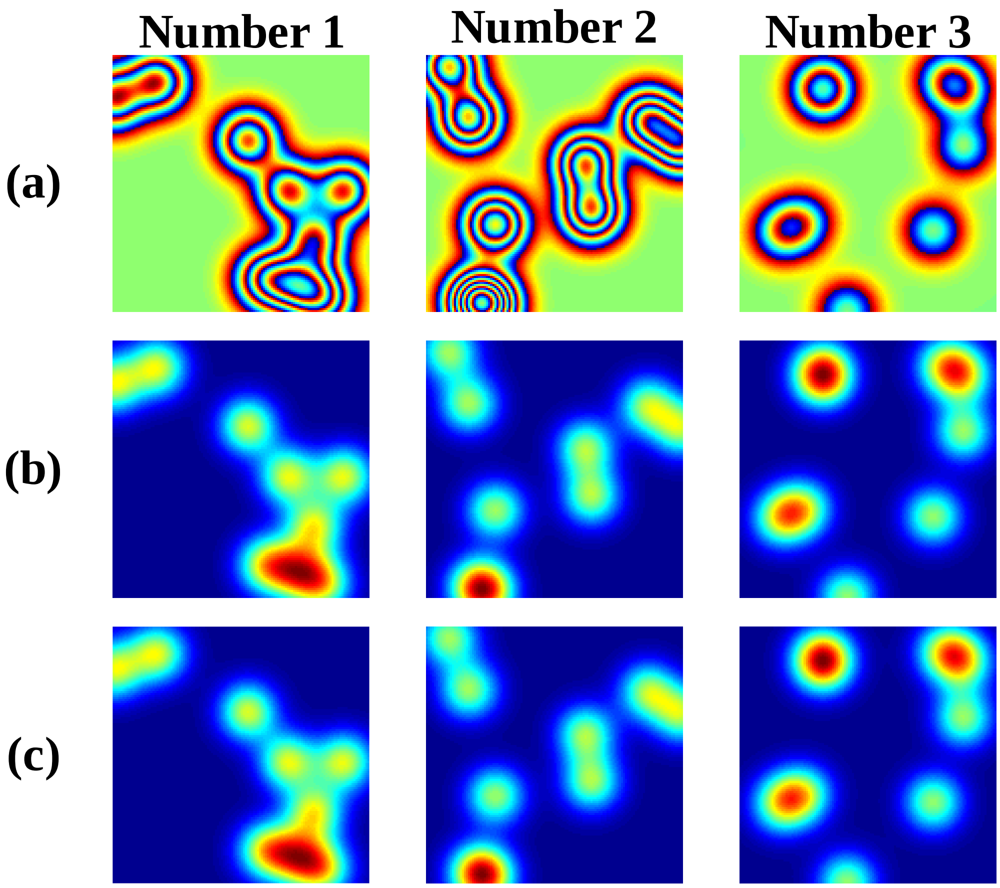

Fig.7. Testing results of phase unwrapping using the SRDU-Net. (a) wrapped phase; (b) true phase; (c) unwrapped phase obtained by SRDU-Net.

Table 3. The values of two metrics for Fig. 7.

Metrics	Number 1	Number 2	Number 3
RMSE	0.0272	0.0162	0.0149
SSIM	0.9889	0.9821	0.9919

3.2 Robustness Testing

In the experiments of collecting holograms, speckle noise is easily generated due to the performance of the optical components and the experimental environment. Therefore, to verify the robustness of the SRDU-Net network, eight sets of simulated data with speckle noise intensity increasing from 0 to 7 with 1 are selected for phase unwrapping using GBC, DCT-LS, Res-UNet network and SRDU-Net network, respectively, and the testing results are shown in Fig. 8.

As can be seen from Fig. 8, the unwrapped phase obtained by GBC has a wide range of phase distortion when the speckle noise intensity is 4. In addition, the unwrapped phase obtained by DCT-LS shows local phase distortion when the speckle noise intensity is 2, and extensive phase distortion when the speckle noise intensity is 3. The unwrapped phase obtained by Res-UNet begins to show phase distortion when the speckle noise intensity is 3, and becomes significant when the intensity is 4. In contrast, the unwrapped phase obtained by SRDU-Net does not begin to show local phase distortion until the speckle noise intensity reaches 7. For a more intuitive comparison of the suppression effects of the four methods on speckle noise, the calculation results for the RMSE and SSIM corresponding to Fig. 8 are shown in Fig. 9, and the mean values of the two metrics are given in Table 4.

It can be observed from Fig. 9 that as the speckle noise intensity increases, the SSIM decrease rate and the RMSE increase rate of SRDU-Net are significantly lower than those of the other three methods. In addition, as can be seen from Table 4, the mean value of RMSE for SRDU-Net is significantly lower than the other three methods, while the mean value of SSIM is significantly higher than them, which shows that the SRDU-Net network proposed in this paper has a strong robustness.

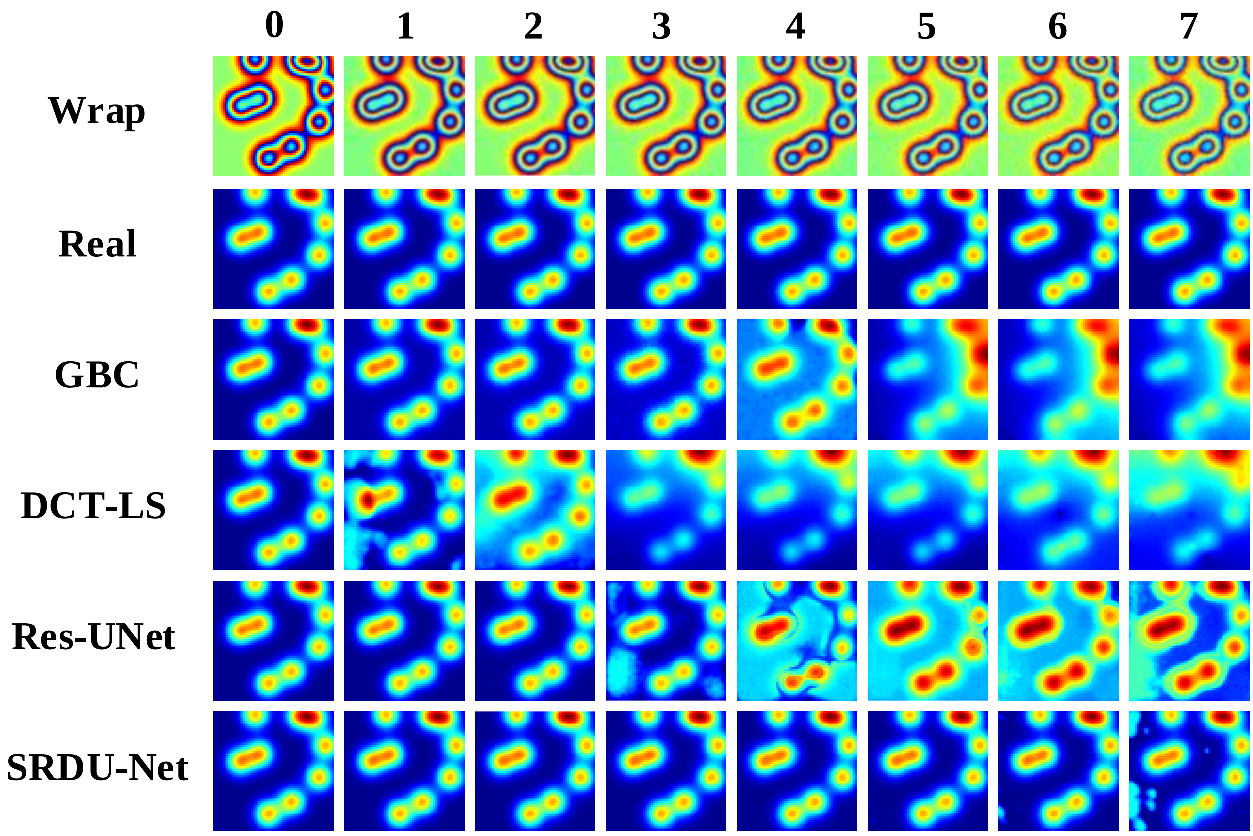

Fig.8. Testing results of phase unwrapping using four methods

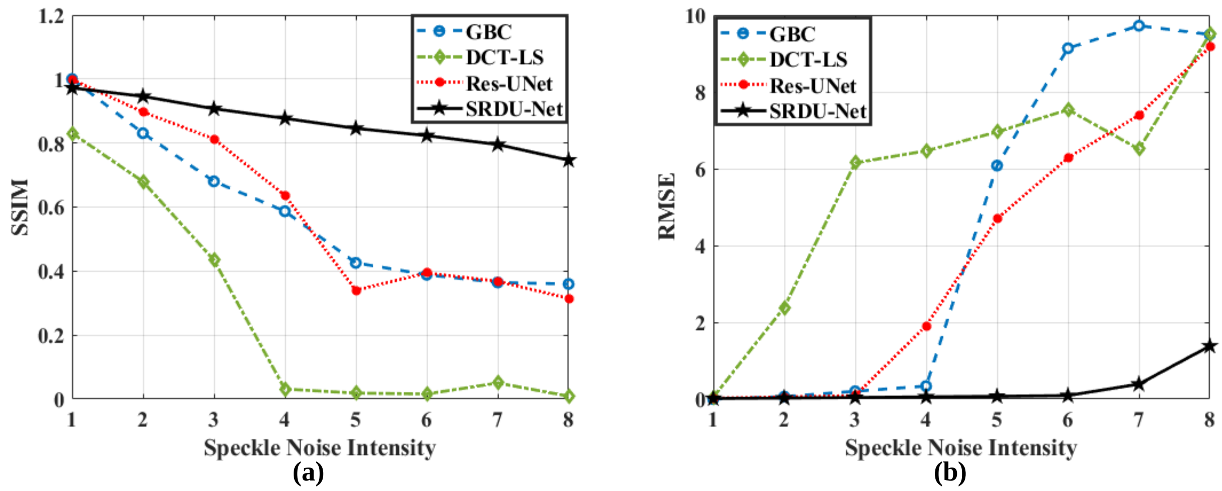

Fig. 9. The calculation results of two metrics for Fig. 8. (a) SSIM; (b) RMSE.

Table 4. The mean values of the two metrics with different methods.

Mean	GBC	DCT-LS	Res-UNet	SRDU-Net
SSIM	0.5795	0.2588	0.5953	**0.8642**
RMSE	4.3797	5.6935	3.7013	**0.2597**

4 Experimental Results and Analysis

4.1 Experimental Setup

To collect the holograms of the test samples, a reflective off-axis digital holographic optical system is constructed in this paper, the experimental setup of which is shown in Fig. 10. A He-Ne laser is used as the light source with a wavelength of 632.8nm. The beam emitted by the laser is reflected twice in succession by the reflectors M1 and M2, and uniformly collimated by the Collimator Beam Expanding System (CBES) and the lens L1. The beam is then reflected by the reflector M3, and split into two beams by the beam splitter BS. The reflected beam is reflected by the surface of the object to form the object light. The transmitted beam is reflected by the reflector M4 to form a reference light. The object and the reference lights interfere at a certain angle on the CCD sensitive surface, and the interference pattern is recorded by the CCD and processed by the computer to form a hologram.

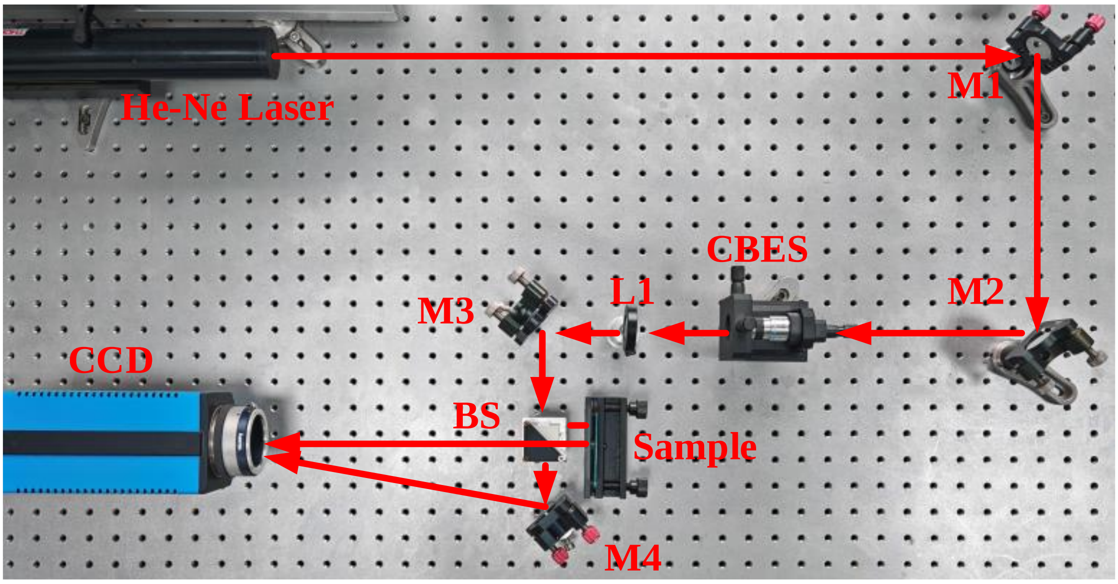

Fig. 10. Experimental setup.

To verify the feasibility and effectiveness of the SRDU-Net network model in digital holographic experiments, the USAF-1951 test target is used as a test sample, as shown in Fig. 11 (a). The holograms of Regions I, II, and III in the rectangular boxes of Fig. 11 (a) are collected by the above experimental setup, i.e., horizontal stripes, vertical stripes, and the number '-2', respectively. In addition, another experiment is carried out using silicon packaging materials marked with ink-dot patterns in Fig. 11(b) to verify the generalization of the proposed method.

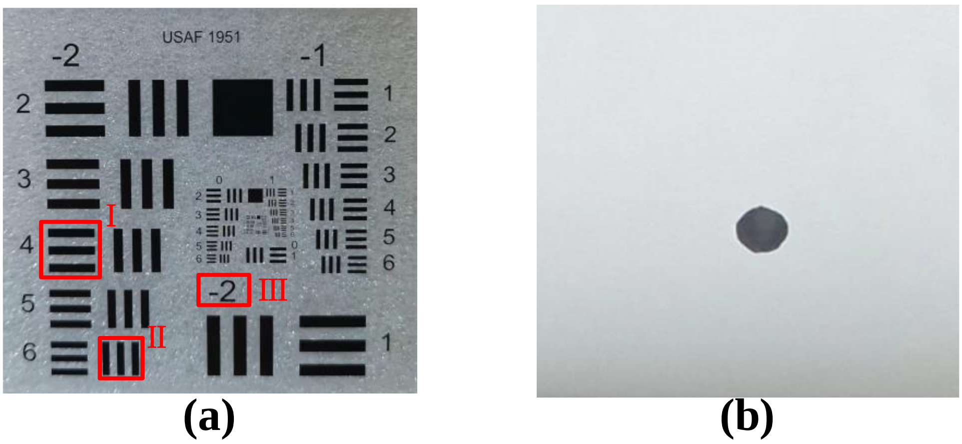

Fig.11. Test samples. (a) USAF-1951 test target; (b) silicon packaging materials marked with ink-dot patterns.

4.2 Testing Results and Discussion

To assess the phase unwrapping performance of the proposed method for the experimental holograms, GBC, DCT-LS, Res-UNet and SRDU-Net are used to unwrap the holograms containing speckle noise.

The experimental results of the hologram of Region I in Fig. 11 (a) are shown in Fig. 12. It can be observed that the SRDU-Net method can effectively separate the phase information of the horizontal stripes from the background with the highest clarity and integrity of the phase information. The edge phase information of all four methods is affected by the edge effect of the CCD sensitive surface, resulting in different degrees of phase distortion, and the Res-UNet has the least phase distortion. In addition, the GBC, DCT-LS and Res-UNet methods all suffer from different degrees of phase distortion due to systematic aberrations, with the SRDU-Net being the least affected, while the SRDU-Net is hardly affected by systematic aberrations. On the other hand, speckle noise causes partial loss of the phase of the third horizontal stripe and mixing of the phase of the second horizontal stripe with the background in the GBC, DCT-LS and Res-UNet methods, especially the unwrapped phase obtained by the GBC method shows multiple phase voids at the second horizontal stripe due to the phase residuals. In particular, the clarity of the second horizontal stripe phase in the DCT-LS method is better than that in the GBC and Res-UNet methods.

The experimental results of region II are shown in Fig.13. It can be seen that the SRDU-Net method still has a superior performance in terms of both the integrity and clarity of the phase information of the vertical fringe. The edge effect of the CCD sensitive surface causes different degrees of phase disturbance in the edge phase information of the four methods, and the Res-UNet has a relatively minimal perturbation. The system distortion causes different degrees of phase distortion in the GBC, DCT-LS and Res-UNet methods, while the SRDU-Net is hardly affected. In addition, speckle noise can cause phase blurring in the lower half part of the vertical stripes for GBC, DCT-LS and Res-UNet. Note that the GBC method produces a phase void in the second vertical fringe due to the influence of the phase residual point.

In order to evaluate the phase unwrapping performance of the proposed method for the detail information of a hologram, the hologram of Region III is performed for phase unwrapping using the above-mentioned four methods, and the experimental results are shown in Fig. 14. It can be observed that the GBC, DCT-LS and Res-UNet methods have different degrees of phase distortion at the image edges, while the SRDU-Net method has some phase perturbations in the phase edge information. Note that the GBC, DCT-LS and Res-UNet methods have different degrees of phase ambiguity in the number '-2 ' part of the unwrapped maps. Obviously, the clarity of the unwrapped phase map obtained by the SRDU-Net is significantly higher than that of the other three methods.

To verify the generalization capability of the proposed method, the wrapped phase map in Fig. 11 (b) is unwrapped using the above four methods, and the experimental results are shown in Fig. 15. It can be seen that due to the influence of residual points, phase voids still appear in the central region for the GBC method. The phase unwrapping results of the other three methods show that SRDU-Net obtains the clearest object phase information.

From the above four experimental results, it can be shown that the GBC method is greatly affected by the phase residual point, and phase voids appear in all four experimental results. The DCT-LS, Res-UNet and SRDU-Net methods are all affected by system aberrations and speckle noise, but the SRDU-Net method has the smallest fluctuation range of the phase height information as well as smaller phase variations, and no phase loss and phase ambiguity appear in the four experimental results, which indicates that the SRDU-Net method has stronger anti-interference ability for system aberrations and speckle noise, so it has better robustness. In addition, both Res-UNet and SRDU-Net methods can obtain the phase information of the experimentally obtained hologram, which shows that both networks have good generalization ability. Thus, the SRDU-Net method shows the object phase with the highest degree of clarity in four experiments, demonstrating that it can achieve high-precision recovery of the wrapped phase of the hologram.

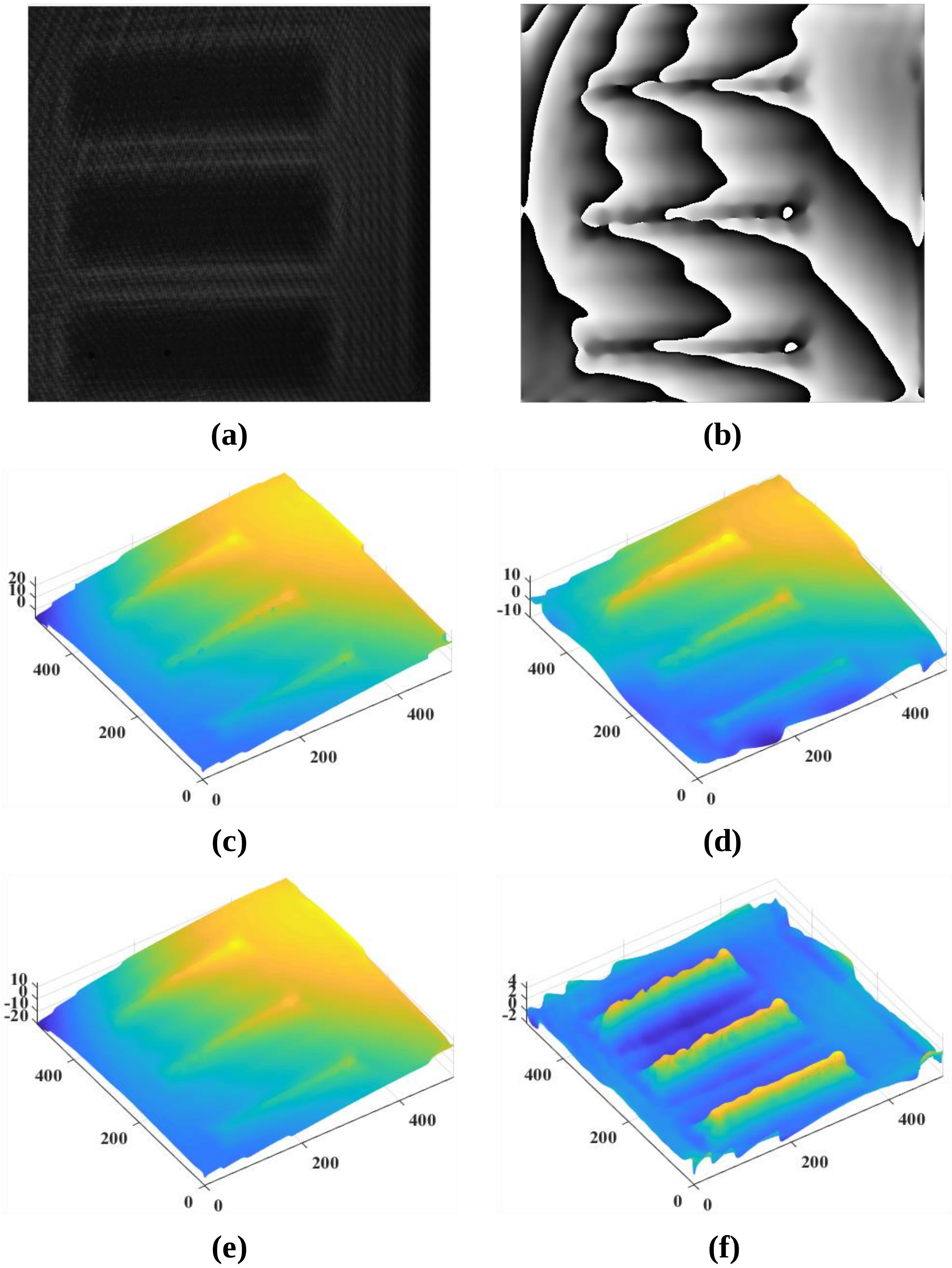

Fig.12. Experimental results of Region I. (a) hologram; (b) wrapped phase map; (c-f) unwrapped phase maps with GBC, DCT-LS, Res-UNet and SRDU-Net.

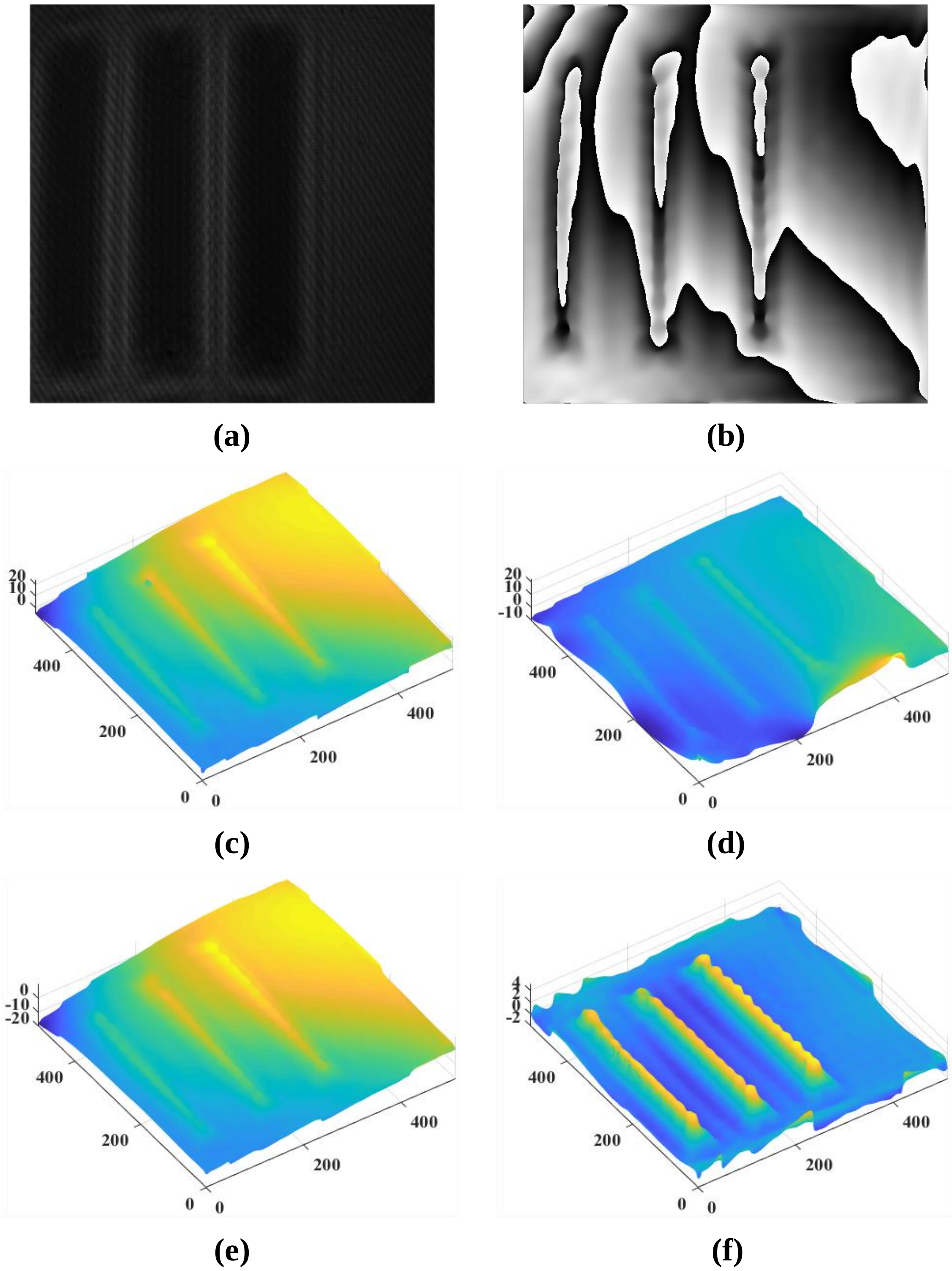

Fig.13. Experimental results of Region II. (a) hologram; (b) wrapped phase map; (c-f) unwrapped phase maps with GBC, DCT-LS, Res-UNet and SRDU-Net.

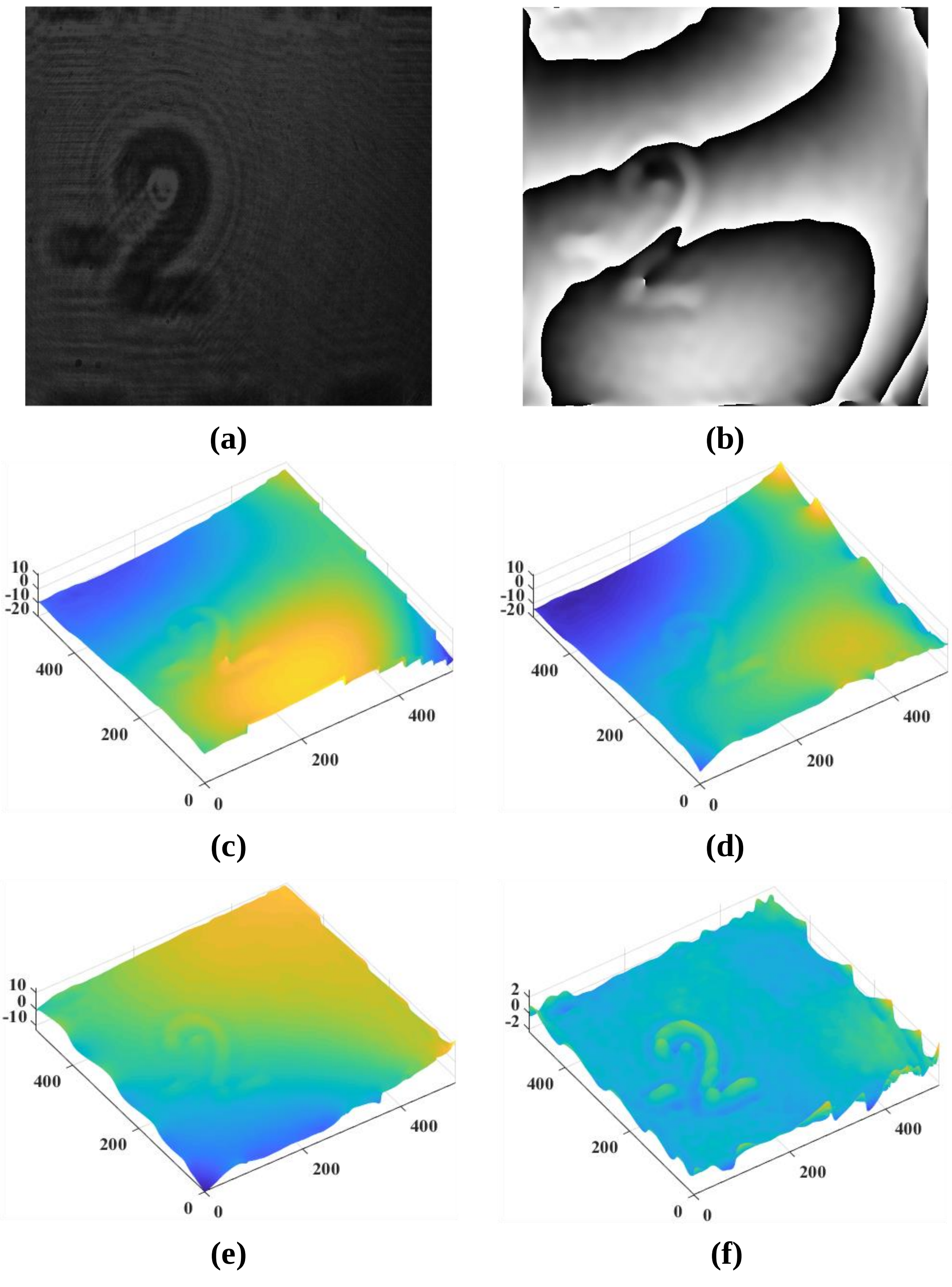

Fig.14. Experimental results of Region III. (a) hologram; (b) wrapped phase map; (c-f) unwrapped phase maps with GBC, DCT-LS, Res-UNet and SRDU-Net.

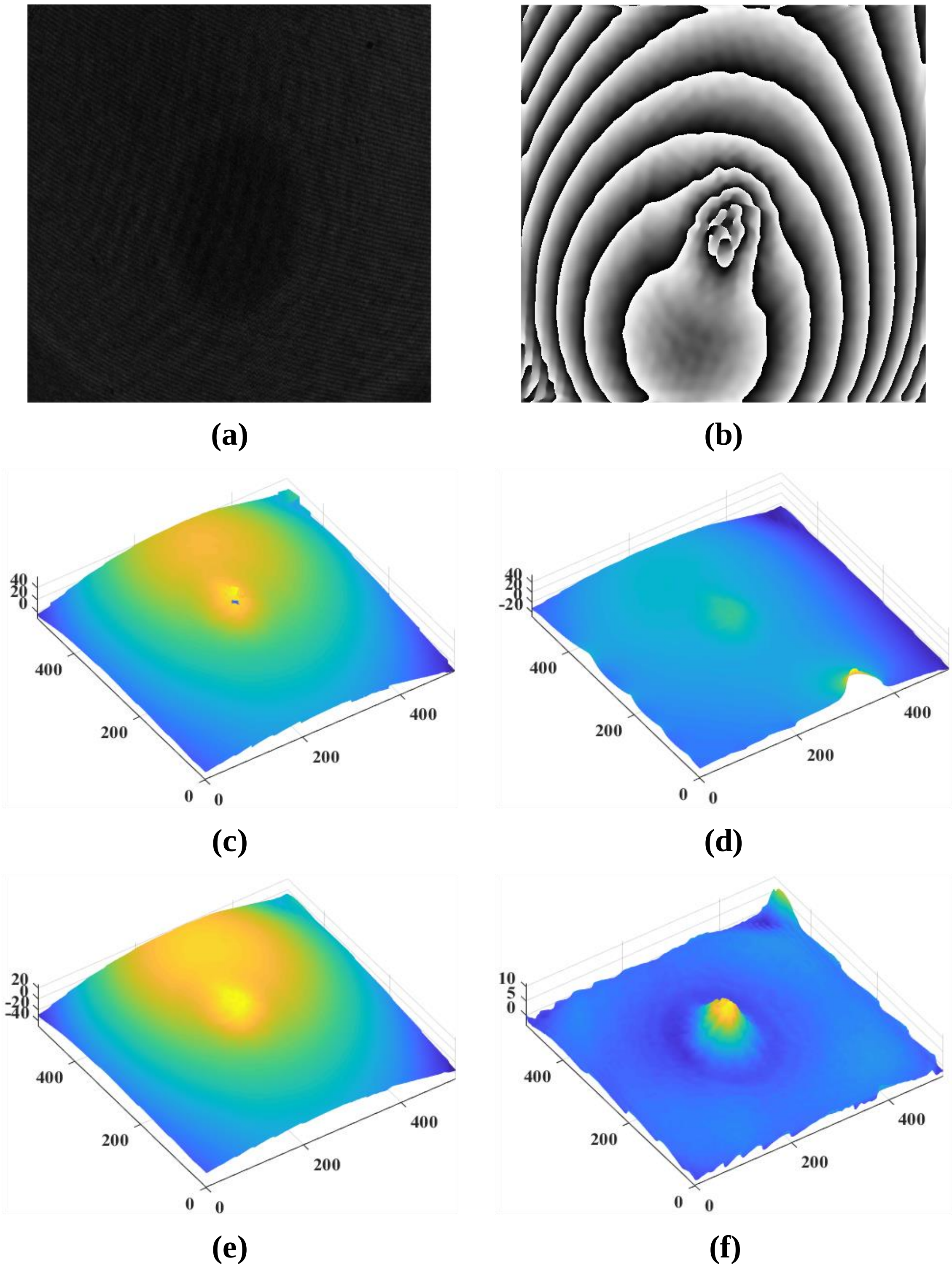

Fig.15. Experimental results for silicon packaging materials marked with ink-dot patterns. (a) hologram; (b) wrapped phase map; (c-f) unwrapped phase maps with GBC, DCT-LS, Res-UNet and SRDU-Net.

5. Conclusions

In this paper, a digital holographic phase unwrapping method based on SRDU-Net was proposed. The simulated phase datasets are randomly generated by both GFS and RME, which are used to train and test the SRDU-Net network. Furthermore, the simulated wrapped phase maps with different levels of speckle noise are used to test the noise immunity of the SRDU-Net, and finally the performance of the proposed method is verified using the holograms of the test samples collected from the experiments. The experimental results show that the proposed SRDU-Net network can recover the wrapped phases with better accuracy and continuity, and achieve the good phase unwrapping results. Moreover, the holograms obtained from the experiments contain some speckle noise and systematic aberration, thus proving that it has a good robustness. In addition, the SRDU-Net method can obtain the phase information of different sample holograms, which indicates that it has a good generalization ability.

Funding. National Natural Science Foundation of China (Grant No. 52175518).

Disclosures. The authors declare no conflicts of interest.

Data availability. Data underlying the results presented in this paper are not publicly available at this time but may be obtained from the authors upon reasonable request.

References

[1] Kim H W, Cho M and Lee M C. A novel image processing method for obtaining an accurate three-dimensional profile of red blood cells in digital holographic microscopy[J]. Biomimetics, 2023, 8(8): 563.

[2] Nagahama Y. Digital holography without a dark room environment: extraction of interference fringes by using deep learning[J]. Applied Optics, 2023, 62(33): 8911-8917.

[3] Kim J, Lee S J. Digital in-line holographic microscopy for label-free identification and tracking of biological cells[J]. Military Medical Research, 2024, 11(1): 38.

[4] Lu X, Xiao X, Xiao W, et al. Screening for urothelial carcinoma cells in urine based on digital holographic flow cytometry through machine learning and deep learning methods[J]. Lab on a Chip, 2024, 24(10): 2736-2746.

[5] Zhang J W, Wang S Q, Li W R, et al. Azimuthal scanning excitation surface plasmon resonance holographic microscopy[J]. Laser & Photonics Reviews, 2024, 4: 2301013.

[6] Bao Q K, Zhang T Y, Liu F H, et al. Phase unwrapping algorithm based on phase edge tracking for dynamic measurement[J]. Optics Express, 2022, 30(5): 7551-7565.

[7] Wu Z J, Guo W B, Zhang Q C. Two-frequency phase-shifting method vs. Gray-coded-based method in dynamic fringe projection profilometry: A comparative review[J]. Optics and Lasers in Engineering, 2022, 153: 106995.

[8] Zuo C, Huang L, Zhang M L, et al. Temporal phase unwrapping algorithms for fringe projection profilometry: A comparative review[J]. Optics and Lasers in Engineering, 2016, 85: 84-103.

[9] Chen J S, Cao Y P, Wu H T. Phase measuring profilometry based on binary grating projection for fringe order self-extraction[J]. Optics Communications, 2022, 517: 128280.

[10] Xu C, Cao Y P, Wu H T, et al. Curtain-type phase unwrapping algorithm[J]. Optical Engineering, 2022, 61(4): 044103.

[11] Zhao Z X, Zhang H Y, Ma C Q, et al. Comparative study of phase unwrapping algorithms based on solving the Poisson equation[J]. Measurement Science and Technology, 2020, 31(6): 065004.

[12] Wang X, Fang S P, Zhu X D, et al. Phase unwrapping based on adaptive image in-painting of fringe patterns in measuring gear tooth flanks by laser interferometry[J]. Optics express, 2020, 28(12): 17881-17897.

[13] Deprem Z and Onat E. Phase unwrapping via hierarchical and balanced residue partitioning[J]. Signal, Image and Video Processing, 2024, 18(3): 2859-2902.

[14] Wang J, Cao Y P, Wu H T, et al. Absolute phase retrieval based on fringe amplitude encoding without any additional auxiliary pattern[J]. Optics Express, 2023, 31(25): 41952-41966.

[15] Wang Y W, Liu L, Wu J, et al. Spatial binary coding method for stripe-wise phase unwrapping[J]. Applied optics, 2020, 59(14): 4729-4285.

[16] Wu H T, Cao Y P, Dai Y B, et al. Orthogonal spatial binary coding method for high-speed 3D measurement[J]. IEEE transactions

on image processing, 2024, 33: 2703-2713.
[17] Ruan G S, Cao Y P, Wu H T, et al. Absolute phase retrieval based on spatial ternary phase coding with circular fringe projection[J]. Optics and Lasers in Engineering, 2024, 178: 108167.
[18] Li F F, Fu Y J, Tian S Y, et al. A two-phase unwrapping three-dimensional measurement method based on phase shift coding[J]. Journal of Modern Optics. 2023, 70(16-18): 929-942.
[19] Zhou H Y, Cheng C L, Peng H, et al. The PHU-NET: A robust phase unwrapping method for MRI based on deep learning[J]. Magnetic Resonance in Medicine, 2021, 86(6): 3321-3333.
[20] Zhou H Y, Yu H W, Pascazio V, et al. PU-GAN: A one-step 2-D InSAR phase unwrapping based on conditional generative adversarial network[J]. IEEE Transactions on Geoscience and Remote Sensing, 2022, 60: 1-10.
[21] Gili D, Nir A. T, Natan T. S. Deep learning approaches for unwrapping phase images with steep spatial gradients: a simulation[C]. IEEE International Conference on the Science of Electrical Engineering in Israel (ICSEE), Eilat, Israel, 12-14 December, 2018.
[22] Zhu W Q and Beroza G C. PhaseNet: A deep-neural-network-based seismic arrival-time picking method[J]. Geophysical Journal International, 2019, 216(1): 261-273.
[23] Spoorthi G E, Rama K S and Gorthi S. PhaseNet 2.0: Phase unwrapping of noisy data based on deep learning approach[J]. IEEE Transactions on Image Processing, 2020, 29: 4862-4872.
[24] Yan K, Yu Y, Sun T, et al. Wrapped phase denoising using convolutional neural networks[J]. Optics and Lasers in Engineering, 2020, 128: 105999.
[25] Wang K Q, Qian K, Di J L, et al. Deep learning spatial phase unwrapping: a comparative review[J]. Advanced Photonics Nexus, 2022, 1(1): 014001
[26] Shah K D, Patel D K, Thaker M P, et al. EMED-UNet: an efficient multi-encoder-decoder based UNet for medical image segmentation[J]. IEEE Access, 2023, 11: 95253-95266.
[27] Wang K, Li Y, Kemao Q, et al. One-step robust deep learning phase unwrapping[J]. Optics Express, 2019, 27(10): 15100-15115.
[28] Xu J, Li Z S, Du B, et al. Reluplex made more practical: Leaky ReLU[C]. 2020 IEEE Symposium on Computers and Communications, Rennes, France, July 7-10, 2020.
[29] Meyer P G. An alternative probabilistic interpretation of the Huber loss [C]. Proceedings of the IEEE/CVF Conference on Computer Vision and Pattern Recognition (CVPR), 2021: 5261-5269.
[30] Wang K Q, Li Y, Ke M Q, et al. One-step robust deep learning phase unwrapping[J]. Optics express, 2019, 27(10): 15100-15115.
[31] Qin Y, Wan S J, Wan Y H, et al. Direct and accurate phase unwrapping with deep neural network[J]. Applied Optics, 2020, 59(24): 7258-7267.
[32] Xu M, Chen T, Shen Y X, et al. PU-M-Net for phase unwrapping with speckle reduction and structure protection in ESPI[J]. Optics and Lasers in Engineering, 2022, 151: 106824.
[33] Wu C C, Qiao Z Y, Zhang N, et al. Phase unwrapping based on a residual en-decoder network for phase images in Fourier domain Doppler optical coherence tomography[J]. Biomedical optics express, 2020, 11(4): 1760-1771.
[34] Sumanth K V, Naveen P, Sai K R G S. 3D deformation measurement in digital holographic interferometry using a multitask deep learning architecture[J]. Journal of the Optical Society of America. A, Optics, image science, and vision, 2022, 39(1): 167-176.
[35] Zhang J K, Li Q G. EESANet: edge-enhanced self-attention network for two-dimensional phase unwrapping[J]. Optics express, 2022, 30(7): 10470-10490.
[36] Zhang J K, Tian X B, Shao J B, et al. Phase unwrapping in optical metrology via denoised and convolutional segmentation networks[J]. Optics express, 2019, 27(10): 14903-14912.
[37] Yan K T, Yu Y J, Sun T, et al. Wrapped phase denoising using convolutional neural networks[J]. Optics and Lasers in Engineering, 2020, 128: 105999.
[38] Gili D, Darina R, K S M, et al. PhUn-Net: ready-to-use neural network for unwrapping quantitative phase images of biological cells[J]. Biomedical optics express, 2020, 11(2): 1107-1121.
[39] Seonghwan P, Youhyun K and Inkyu M. Automated phase unwrapping in digital holography with deep learning[J]. Biomedical optics express, 2021, 12(11):7064-7081.

[40] Cheremkhin P A, Evtikhiev N N, Kozlov A V, et al. An optical-digital method of noise suppression in digital holography[J]. Journal of Optics, 2022, 24(11): 115702.

[41] Yan L P, Wang Q X, Liu H, et al. Phase unwrapping of digital holographic microscopy using adaptive region segmentation and phase derivative calibration with respect to fringe density[J]. Optics and Lasers in Engineering, 2022, 148: 106780.